



Asymmetry in the climate–carbon cycle response to positive and negative CO₂ emissions

Kirsten Zickfeld¹✉, Deven Azevedo¹, Sabine Mathesius¹ and H. Damon Matthews^{1,2}

Negative CO₂ emissions are a key mitigation measure in emission scenarios consistent with temperature limits adopted by the Paris Agreement. It is commonly assumed that the climate–carbon cycle response to a negative CO₂ emission is equal in magnitude and opposite in sign to the response to an equivalent positive CO₂ emission. Here we test the hypothesis that this response is symmetric by forcing an Earth system model with positive and negative CO₂ emission pulses of varying magnitude and applied from different climate states. Results indicate that a CO₂ emission into the atmosphere is more effective at raising atmospheric CO₂ than an equivalent CO₂ removal is at lowering it, with the asymmetry increasing with the magnitude of the emission/removal. The findings of this study imply that offsetting positive CO₂ emissions with negative emissions of the same magnitude could result in a different climate outcome than avoiding the CO₂ emissions.

The majority of emissions scenarios consistent with the objective of the Paris Agreement of limiting global mean warming ‘to well below 2 °C above pre-industrial levels and pursuing efforts to limit warming to 1.5 °C’ include net negative emissions in the second half of this century^{2,3}, that is, artificial CO₂ removal from the atmosphere at a level that exceeds CO₂ emissions. Yet, only a few studies have explored the Earth system response to net negative emissions^{4–8}. Understanding how the coupled climate–carbon cycle (C–CC) responds to net negative CO₂ emissions is key to evaluating the effectiveness of negative emissions technologies at lowering atmospheric CO₂^{5,6}. A common assumption is that the C–CC response is symmetric, such that the C–CC response to a negative CO₂ emission is equal in magnitude and opposite in sign to the response to a positive CO₂ emission. For example, in emissions scenarios, a positive CO₂ emission is usually offset exactly by a negative emission, implicitly assuming symmetry in terms of their climate outcomes³. While reasonable for a small emission (on the order of 1 GtC), this assumption is questionable for larger emissions comparable to the size of the anthropogenic perturbation (on the order of 100 GtC) due to non-linearities and state dependencies in the C–CC response to CO₂ emissions. Here, we evaluate the symmetry in the carbon cycle and surface air temperature response to negative and positive CO₂ emission pulses of different magnitude and applied from different climate states.

We conduct and analyse simulations with the University of Victoria Earth System Climate Model (UVic ESCM 2.9)^{9,10}, an Earth system model of intermediate complexity. The model is forced with either a positive or negative instantaneous CO₂ emission (‘pulse’) in the range from ±100 to ±1,000 GtC (±100, ±200, ±500 or ±1,000 GtC). Negative emission pulses of –100 to –500 GtC are broadly consistent with the range of total net negative emissions of 130–430 GtC by year 2200 in extended Shared Socio-economic Pathways (SSPs) with negative emissions (SSP1-1.9, SSP1-2.6, SSP5-3.4 and SSP4-3.4)¹¹, while the –1,000 GtC pulse lies outside of this range. We nevertheless include it as an extreme case and for comparison with literature on positive CO₂ emission pulses that has evaluated the response to a 1,000 GtC pulse¹². CO₂ emission pulses are applied from model states in equilibrium with different

atmospheric CO₂ levels (1×, 1.5×, 2×, 3× and 4× the pre-industrial CO₂ concentration). In the case of negative emissions, CO₂ is removed directly from the atmosphere and taken out of the system permanently, similar to the process of direct air carbon capture and storage (DACCs)¹³. No forcing other than CO₂ is applied (see Methods for further details). We apply the emission pulses from a state of equilibrium rather than a transient trajectory to clearly isolate the response to the emission pulse from the response to the prior forcing trajectory. This is particularly important for negative emission pulses, as the response to such pulses applied from a transient state is a combination of the response to the prior (positive) forcing trajectory and the response to the negative emission¹⁴, and differs substantially from the response to a pulse applied from an equilibrium state (Supplementary Fig. 1).

The atmospheric CO₂ concentration declines rapidly and then rebounds in response to negative CO₂ emission pulses (Fig. 1a). The atmospheric CO₂ rebound is due to CO₂ release by the terrestrial biosphere and the ocean in response to declining atmospheric CO₂ levels. Land CO₂ release peaks a few years after the pulse and then decreases, switching to net CO₂ uptake within 50 years of the pulse removal (Fig. 1c). This response reflects the different response timescales of the processes driving the exchange of CO₂ between the land and the atmosphere: net primary productivity (NPP) declines quickly in response to decreasing atmospheric CO₂, while soil respiration declines more slowly in response to decreasing surface air temperature (Extended Data Fig. 1). Initially, the decline in NPP exceeds the decline in soil respiration, resulting in rapid CO₂ loss from the land carbon pool. After a few decades, the decline in soil respiration exceeds the decline in NPP and the land turns into a weak CO₂ sink, regaining part of the lost CO₂. Ocean CO₂ release reaches its maximum a few years after the pulse and then declines, resulting in continuous loss of CO₂ from the ocean pool (Fig. 1d). On timescales <100 years, CO₂ is released primarily from the ocean mixed layer, whereas on longer timescales, CO₂ is released from the deep ocean, driven by the negative CO₂ gradient at the sea surface (higher CO₂ partial pressure at the sea surface than in the atmosphere). The amplitude of the land and ocean response increases with increasing negative CO₂ emission pulses (Fig. 1c,d). The more

¹Department of Geography, Simon Fraser University, Burnaby, British Columbia, Canada. ²Department of Geography, Planning and Environment, Concordia University, Montreal, Quebec, Canada. ✉e-mail: kzickfel@sfu.ca

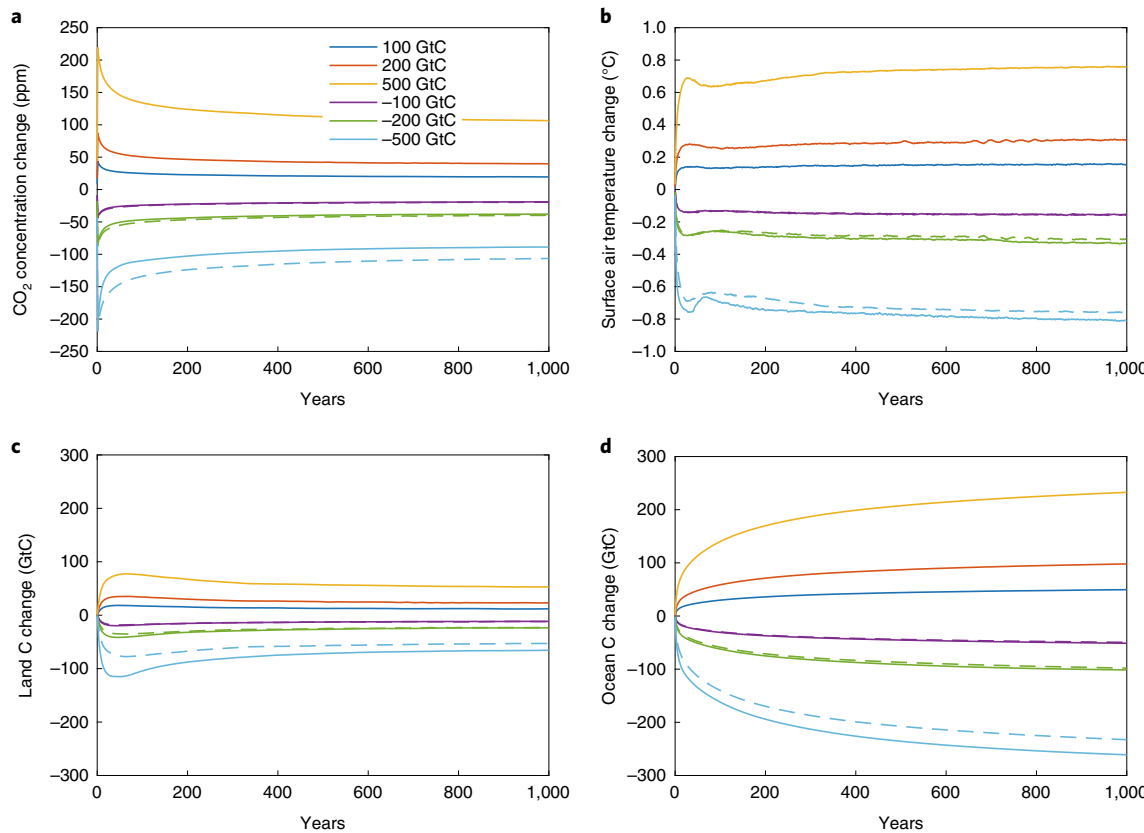


Fig. 1 | Simulated carbon cycle and surface air temperature response to positive and negative CO₂ emission pulses. **a–d**, Atmospheric CO₂ concentration anomaly (**a**), surface air temperature anomaly (**b**), land carbon storage change (**c**) and ocean carbon storage change (**d**) calculated relative to a control simulation with zero CO₂ emissions initialized from the 2×CO₂ equilibrium state. Dashed lines show the response to positive CO₂ emission pulses mirrored about the horizontal zero line to illustrate the asymmetry in the responses.

CO₂ that is removed from the atmosphere, the larger the imbalance between changes in NPP and soil respiration, and the larger the negative CO₂ gradient at the sea surface, resulting in a larger CO₂ release to the atmosphere. The C–CC response under positive CO₂ emissions has been studied extensively¹⁵ and will not be discussed here.

The atmospheric CO₂ response to positive and negative CO₂ emission pulses of equal magnitude is asymmetric, particularly for larger (>100 GtC) pulses (compare the dashed and solid lines in the lower half of Fig. 1a). The magnitude of the initial CO₂ response is slightly larger for positive CO₂ pulses, but the rebound is less pronounced. This asymmetry in the atmospheric CO₂ response is due to asymmetries in the response of land and ocean CO₂ fluxes. Initially (<100 years), the asymmetry in atmospheric CO₂ is largely caused by asymmetry in land CO₂ uptake/release (Fig. 1c,d). After about 50 years, the asymmetry in the land response decreases, and after about 200 years, asymmetry in ocean CO₂ uptake/release becomes dominant. For both land and ocean CO₂ fluxes, the magnitude of the response to negative pulses is larger than that to positive pulses. These asymmetries are associated with non-linearities in the response of land and ocean CO₂ fluxes to atmospheric CO₂ and climate changes, as discussed below.

The asymmetry in the C–CC response is also evident in the fractional changes in atmosphere, land and ocean carbon reservoirs for negative and positive CO₂ emission pulses (Fig. 2). For negative CO₂ emission pulses, we refer to the fractional change in the atmosphere carbon (C) burden as the cumulative removal fraction (CRF), equivalently to the cumulative airborne fraction (CAF) for positive CO₂

emissions. The CAF is 0.53 and the CRF is 0.51 at 100 years after a positive and negative 100 GtC pulse applied from a 2×CO₂ equilibrium, respectively, indicating that a positive emission is slightly more effective at raising atmospheric CO₂ than a negative emission of the same magnitude is at lowering it. This asymmetry increases with the size of the emission/removal: for a 500 GtC pulse applied from 2×CO₂ the CAF is 0.57 whereas the CRF is 0.47, meaning that 57% of a positive 500 GtC emission remains airborne, whereas only 47% of a 500 GtC removal remains out of the atmosphere. This asymmetry in the cumulative airborne/removal fraction is a result of asymmetries in the land and ocean CO₂ uptake/release fractions (Fig. 2b,c). The ocean and land CO₂ release fractions are larger for negative CO₂ emission pulses than the CO₂ uptake fractions, with the asymmetry increasing with pulse size. The decrease in land and ocean CO₂ uptake fraction with larger positive CO₂ emissions is consistent with earlier studies^{16,17}. The asymmetry in the climate–carbon response is robust with respect to the initial atmospheric CO₂ concentration from which the pulse is applied (CO₂¹⁰) (Fig. 2). For CO₂¹⁰ ranging from 1× to 4× the pre-industrial CO₂ concentration, the CAF is consistently larger than the CRF, with the difference increasing with the size of the emission/removal (Fig. 2a).

The asymmetry in the land and ocean CO₂ uptake/release is caused by non-linearities in the response to CO₂ and carbon–climate feedbacks. On land, the larger response under negative pulses is largely associated with a declining effectiveness of CO₂ fertilization at higher atmospheric CO₂ levels¹⁸. Because of this non-linear relationship, a CO₂ removal will result in a larger CO₂ response than an emission of the same magnitude. In the ocean, asymmetry in CO₂

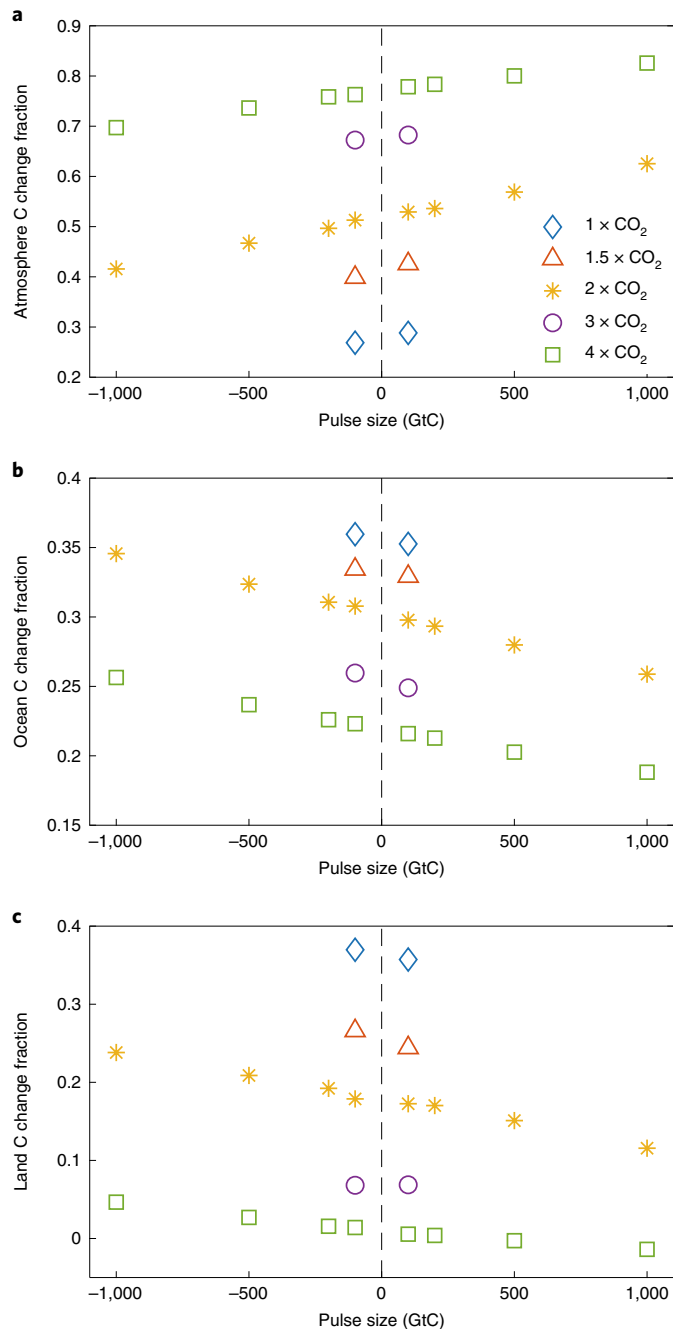


Fig. 2 | Changes in carbon stores as a fraction of cumulative CO_2 emissions and removals (equivalent to CO_2 pulse size) 100 years after pulse release for simulations initialized from different equilibrium states ($1 \times \text{CO}_2$ to $4 \times \text{CO}_2$). **a,** Atmospheric carbon burden change fraction. **b,** Ocean carbon store change fraction. **c,** Land carbon store change fraction. Changes in carbon stores are positive (that is, uptake) for positive CO_2 pulses and negative (that is, release) for negative CO_2 pulses, resulting in a positive change fraction in both cases (except for the land carbon change fraction for positive CO_2 pulses initialized from a $4 \times \text{CO}_2$ state, which is negative due to land carbon loss in response to these pulses). Changes are calculated relative to a control simulation with zero CO_2 emissions initialized from the respective equilibrium state.

uptake/release is caused about equally by the asymmetric response to CO_2 and asymmetries in climate feedbacks (Supplementary Table 1). It is well known that the buffer capacity of CO_2 in seawater

decreases non-linearly with CO_2 partial pressures ($p\text{CO}_2$) at the sea surface (Extended Data Fig. 2). Due to this non-linearity, a CO_2 removal results in a larger air-sea CO_2 flux to balance the change in atmospheric CO_2 than a CO_2 emission of the same magnitude. This asymmetric response to CO_2 is amplified by asymmetries in climate feedbacks. The meridional overturning circulation (MOC) strengthens more for negative pulses than it weakens for positive pulses (Extended Data Fig. 3). This asymmetric MOC response results in larger carbon release under negative pulses than carbon uptake under positive pulses, particularly in the North Atlantic and Southern Ocean (Supplementary Fig. 2). This asymmetry in the carbon cycle response to MOC changes is countered to some extent by the saturation of CO_2 solubility with increasing seawater temperature¹⁹. Due to this non-linear dependence, solubility increases more under a negative pulse than it decreases under a positive pulse. This, in turn, leads to a larger increase in the ability of the ocean to take up CO_2 under negative pulses than to release CO_2 under positive pulses. The asymmetric MOC response to positive and negative CO_2 emission pulses may be model dependent, and we expect asymmetry in the ocean carbon cycle response resulting from direct CO_2 effects to be more robust than asymmetry resulting from the interaction of MOC and solubility changes.

To determine the contributions of asymmetric responses to CO_2 and climate change to the total asymmetry, we conducted a set of biogeochemically coupled (but radiatively decoupled) model simulations, whereby the ocean and the terrestrial biosphere ‘see’ an increase in atmospheric CO_2 but do not experience CO_2 -induced climate change (Methods). These simulations reveal that, 100 years after a ± 500 GtC pulse, 87% of the total asymmetry in the land C reservoir change (-25.1 out of -28.9 GtC) and 52% of the asymmetry in the ocean C reservoir change (-11.4 out of -21.9 GtC) are present in the biogeochemically coupled simulation (Supplementary Table 1 and Extended Data Fig. 4). These results suggest that, 100 years after the pulse, emission/release asymmetries in biogeochemical feedbacks dominate the asymmetry in the land response, whereas asymmetry in biogeochemical and climate feedbacks contribute equally to the asymmetry in the ocean response.

For a given pulse size, the cumulative airborne/removal fraction increases significantly at higher initial CO_2 concentrations CO_2^{10} , while the land and ocean C change fractions decrease at higher CO_2^{10} (Fig. 2). For instance, the CAF (CRF) increases from 0.29 (0.27) for CO_2^{10} of $1 \times \text{CO}_2$ to 0.78 (0.76) for CO_2^{10} of $4 \times \text{CO}_2$ for a 100 GtC pulse emission (removal). The decrease in the land and ocean CO_2 uptake/release fractions with increasing CO_2^{10} is again due to non-linearities in the climate–carbon response. The processes driving the weaker land and ocean carbon CO_2 uptake at higher CO_2^{10} are investigated for pulses applied from a $4 \times \text{CO}_2$ state and compared with processes driving the response to pulses applied from a $2 \times \text{CO}_2$ state. The weaker land CO_2 uptake for a positive pulse applied from a $4 \times \text{CO}_2$ state (Fig. 2c) is largely driven by the reduced effectiveness of the CO_2 fertilization effect at higher atmospheric CO_2 concentration, which results in reduced NPP, reduced gain in vegetation carbon and loss in soil carbon (see Supplementary Text and Extended Data Fig. 5–9 for more details). The release of CO_2 from the land in response to negative emission pulses is also reduced for a $4 \times \text{CO}_2$ relative to a $2 \times \text{CO}_2$ state due to the non-linearity in the CO_2 fertilization effect. This non-linearity results in a weaker decline in NPP and reduced loss in vegetation carbon, which is partly offset by gain in soil carbon (Supplementary Text and Extended Data Fig. 6–9). In the ocean, reduced buffer capacity, weaker meridional overturning circulation and stronger temperature stratification at higher CO_2^{10} cause the reduced CO_2 uptake for positive emission pulses. For negative pulses, these same processes hamper the ocean release of CO_2 at higher CO_2^{10} . Due to the non-linear dependence of the buffer capacity on $p\text{CO}_2$, CO_2 removal from a $4 \times \text{CO}_2$ state results in a weaker increase in buffer capacity and hence reduced outgassing

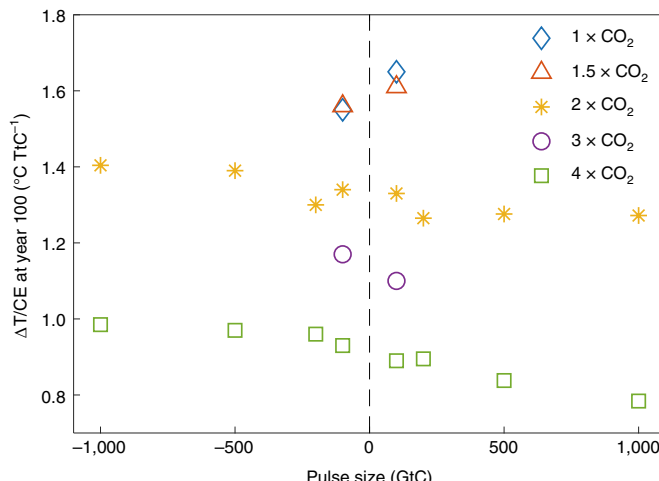


Fig. 3 | Surface air temperature change (ΔT) as a fraction of cumulative CO_2 emissions or removals (CE; equivalent to CO_2 pulse size) 100 years after the pulse release for simulations initialized from different equilibrium states ($1\times\text{CO}_2$ to $4\times\text{CO}_2$). Changes are calculated relative to a control simulation with zero CO_2 emissions initialized from the respective equilibrium state.

than a removal from a $2\times\text{CO}_2$ state (Supplementary Fig. 3). This effect is amplified by a weaker meridional overturning circulation and stronger stratification, which inhibit upward mixing of CO_2 from deeper ocean layers (Supplementary Figs. 4 and 5).

As the majority of climate change impacts are related to surface air temperature (SAT) changes rather than changes in atmospheric CO_2 , the question arises whether the asymmetry in the carbon cycle response to positive and negative CO_2 emission pulses propagates onto asymmetry in temperature changes. Figure 1 indicates that, for emission pulses applied from a $2\times\text{CO}_2$ state, the SAT response is asymmetric (Fig. 1b, compare dashed and solid lines in the lower figure half), although in relative terms the asymmetry is not as pronounced as for atmospheric CO_2 and the sign of the asymmetry is reversed (the SAT response is larger for negative pulses). Figure 3 displays the ratio of SAT anomaly to cumulative CO_2 emissions, a metric related to the transient climate response to cumulative CO_2 emissions (TCRE) for positive CO_2 emissions^{20–22}. Here, we refer to this metric 100 years after the pulse release as TCRR₁₀₀ and the equivalent metric for the climate response to negative emissions as the transient climate response to cumulative CO_2 removals at year 100 (TCRR₁₀₀). For emission pulses applied from a $2\times\text{CO}_2$ initial state, the TCRR₁₀₀ is slightly larger than the TCRE₁₀₀, implying that negative emissions are slightly more effective at cooling than positive emissions are at warming, despite the opposite asymmetry of the CAF and CRF. Asymmetry of the same sign ($\text{TCRR}_{100} > \text{TCRE}_{100}$) is found for emission pulses applied from other initial states, except for the ± 100 GtC pulses applied from $1\times\text{CO}_2$ and $1.5\times\text{CO}_2$ states, which exhibit temperature variability that is relatively large compared with the signal from the pulse release (Extended Data Fig. 10). The TCRE₁₀₀ decreases slightly with emission pulse size (for example, from $1.33^\circ\text{C TtC}^{-1}$ for a 100 GtC pulse to $1.27^\circ\text{C TtC}^{-1}$ for a 1,000 GtC pulse applied from a $2\times\text{CO}_2$ state), consistent with earlier studies with models of intermediate complexity^{23,24}, while the TCRR₁₀₀ increases slightly with pulse size (from $1.34^\circ\text{C TtC}^{-1}$ for a -100 GtC pulse to $1.40^\circ\text{C TtC}^{-1}$ for a $-1,000$ GtC pulse applied from a $2\times\text{CO}_2$ state). TCRE₁₀₀ and TCRR₁₀₀ for ± 200 GtC pulses applied from a $2\times\text{CO}_2$ state are smaller than for both ± 100 GtC and ± 500 GtC pulses applied from the same state because the warming/cooling reaches a relative minimum 100 years after the pulse release (Fig. 1b). The opposite pulse-size dependence of the TCRE₁₀₀ and

TCRR₁₀₀ is an expression of asymmetry. This asymmetry is a result of the logarithmic dependence of radiative forcing on atmospheric CO_2 concentration, such that the radiative forcing change per unit CO_2 change is smaller for positive than negative pulses. This effect results in a smaller temperature response to emissions than to removals even if the CAF is larger than the CRF. It is noteworthy that the TCRE₁₀₀ and TCRR₁₀₀ are substantially smaller for higher initial CO_2 levels, despite significantly larger cumulative airborne/removal fractions (Fig. 2a). This is again due to the logarithmic dependence of radiative forcing on atmospheric CO_2 and the smaller climate sensitivity (temperature change per unit radiative forcing) exhibited by the UVic ESCM at higher atmospheric CO_2 concentrations^{25,26}.

In this study, positive and negative CO_2 emission pulses are applied from an equilibrium climate state to isolate the effect of negative emissions on the coupled climate–carbon system. By letting the model equilibrate with a higher atmospheric CO_2 concentration ($1.5\times$ to $4\times$ the pre-industrial CO_2 concentration), however, the marine and terrestrial carbon sinks are closer to saturation than in a real-world situation where CO_2 emissions are applied from a transient state, which could affect the symmetry in the response. To test the robustness of our results, we conducted an additional set of model simulations whereby emission pulses were applied from a transient trajectory with atmospheric CO_2 increasing at 1% per year up to $2\times$ pre-industrial CO_2 levels (Methods). The response to the negative emission pulses was isolated from the response to the increasing atmospheric CO_2 concentration prior to the pulse release by calculating the difference relative to a zero emission simulation (Methods). Results from this additional analysis suggest that the asymmetry in the C–CC response remains present in model simulations with emission pulses applied from a transient trajectory (Supplementary Fig. 6).

This study investigates the C–CC response to pulse CO_2 emissions, a design that has proven useful to probe the response of the carbon cycle to positive CO_2 emissions¹². The century-timescale climate–carbon response has been shown to be largely path independent^{23,27}, so it is reasonable to expect that the asymmetry in the response also applies to scenarios with more realistic emission/removal rates. We demonstrate that the asymmetry is indeed path independent by showing that the C–CC response for instantaneous (pulse) emissions is very similar to the century-scale response in simulations with the same cumulative emissions/removals applied at ± 10 GtC per year (Methods and Supplementary Fig. 7).

Our results indicate that, 100 years after a pulse emission/removal, about 60% of the asymmetry in the atmospheric CO_2 response to positive and negative emission pulses is due to asymmetry in the land response. The land response to CO_2 and climate change is found to be strongly model dependent^{28,29}, so we expect the magnitude and potentially the sign of the asymmetry to vary across models. On multi-century timescales, the asymmetry in the ocean response becomes dominant, and since the ocean carbon cycle response is less model dependent^{28,29}, we expect the asymmetry to be more robust across models on those timescales. Representation of permafrost carbon and nitrogen limitation, which are not included in the model used for this study, could affect the symmetry in the land carbon cycle response. Translation of the symmetry in the carbon cycle response to temperature asymmetry could also be affected by physical feedback such as cloud feedbacks, which are not represented in the UVic ESCM. A model experiment designed to explore the symmetry in the coupled C–CC response is included in the experimental protocol of the Carbon Dioxide Model Intercomparison Project (CDR-MIP)³⁰, which is part of the Sixth Phase of the Coupled Model Intercomparison Project (CMIP6)³¹. With this concerted modelling effort, it will be possible to investigate the extent to which the asymmetry found in our study is robust across a hierarchy of models with representation of different processes, including cloud feedbacks, permafrost carbon and nitrogen limitation.

This study demonstrates that an emission of CO₂ into the atmosphere is more effective at raising atmospheric CO₂ than a CO₂ removal is at lowering atmospheric CO₂, indicating that the carbon cycle response is asymmetric. This asymmetry increases with the magnitude of the emission/removal. This result implies that an extra amount of CO₂ removal is required to compensate for an emission of a given magnitude to attain the same atmospheric CO₂ concentration. The asymmetry in the global mean temperature response is smaller than the atmospheric CO₂ asymmetry in relative terms and of opposite sign, with a stronger cooling for a removal than warming for an equivalent emission. The findings of this study suggest that offsetting positive CO₂ emissions on the order of 100 GtC with CO₂ removals of the same magnitude could result in a different climate outcome than avoiding the CO₂ emissions.

Online content

Any methods, additional references, Nature Research reporting summaries, source data, extended data, supplementary information, acknowledgements, peer review information; details of author contributions and competing interests; and statements of data and code availability are available at <https://doi.org/10.1038/s41558-021-01061-2>.

Received: 21 December 2019; Accepted: 29 April 2021;

Published online: 21 June 2021

References

1. Adoption of the Paris Agreement FCCC/CP/2015/L.9/Rev.1 (UNFCCC, 2015).
2. Fuss, S. et al. Betting on negative emissions. *Nat. Clim. Change* **4**, 850–853 (2014).
3. Rogelj, J. et al. Scenarios towards limiting global mean temperature increase below 1.5°C. *Nat. Clim. Change* **8**, 325–332 (2018).
4. Cao, L. & Caldeira, K. Atmospheric carbon dioxide removal: long-term consequences and commitment. *Environ. Res. Lett.* **5**, 24011 (2010).
5. Tokarska, K. & Zickfeld, K. The effectiveness of net negative carbon dioxide emissions in reversing anthropogenic climate change. *Environ. Res. Lett.* **10**, 94013 (2015).
6. Jones, C. D. et al. Simulating the Earth system response to negative emissions. *Environ. Res. Lett.* **11**, 095012 (2016).
7. Vichi, M., Navarra, A. & Fogli, P. G. Adjustment of the natural ocean carbon cycle to negative emission rates. *Clim. Change* **118**, 105–118 (2013).
8. Mathesius, S., Hofmann, M., Caldeira, K. & Schellnhuber, H. J. Long-term response of oceans to CO₂ removal from the atmosphere. *Nat. Clim. Change* **5**, 1107–1114 (2015).
9. Weaver, A. J. et al. The UVic earth system climate model: model description, climatology, and applications to past, present and future climates. *Atmos. Ocean* **39**, 361–428 (2001).
10. Eby, M. et al. Lifetime of anthropogenic climate change: millennial time scales of potential CO₂ and temperature perturbations. *J. Clim.* **22**, 2501–2511 (2009).
11. Meinshausen, M. et al. The shared socio-economic pathway (SSP) greenhouse gas concentrations and their extensions to 2500. *Geosci. Model Dev.* **13**, 3571–3605 (2020).
12. Joos, F. et al. Carbon dioxide and climate impulse response functions for the computation of greenhouse gas metrics: a multi-model analysis. *Atmos. Chem. Phys.* **13**, 2793–2825 (2013).
13. Sanz-Pérez, E. S., Murdock, C. R., Didas, S. A. & Jones, C. W. Direct capture of CO₂ from ambient air. *Chem. Rev.* **116**, 11840–11876 (2016).
14. Zickfeld, K., MacDougall, A. H. & Matthews, H. D. On the proportionality between global temperature change and cumulative CO₂ emissions during periods of net negative CO₂ emissions. *Environ. Res. Lett.* **11**, 055006 (2016).
15. IPCC Climate Change 2013: The Physical Science Basis (eds Stocker, T. F. et al.) (Cambridge Univ. Press, 2013).
16. Zickfeld, K. et al. Long-term climate change commitment and reversibility: an EMIC intercomparison. *J. Clim.* **26**, 5782–5809 (2013).
17. Jones, C. et al. Twenty-first-century compatible CO₂ emissions and airborne fraction simulated by CMIP5 Earth system models under four representative concentration pathways. *J. Clim.* **26**, 4398–4413 (2013).
18. Chapin F. S. III & Eviner V. T. in *Treatise on Geochemistry* 2nd edn. (eds Holland H. D. & Turekian K. K.) 189–216 (Elsevier, 2014).
19. Duan, Z. H. & Sun, R. An improved model calculating CO₂ solubility in pure water and aqueous NaCl solutions from 273 to 533 K and from 0 to 2000 bar. *Chem. Geol.* **193**, 257–271 (2003).
20. Matthews, H. D., Gillett, N. P., Stott, P. A. & Zickfeld, K. The proportionality of global warming to cumulative carbon emissions. *Nature* **459**, 829–832 (2009).
21. Gillett, N. P., Arora, V. K., Matthews, D. & Allen, M. R. Constraining the ratio of global warming to cumulative CO₂ emissions using CMIP5 simulations. *J. Clim.* **26**, 6844–6858 (2013).
22. Collins, M. et al. in *Climate Change 2013: The Physical Science Basis* (eds Stocker, T. F. et al.) (Cambridge Univ. Press, 2013).
23. Herrington, T. & Zickfeld, K. Path independence of climate and carbon cycle response over a broad range of cumulative carbon emissions. *Earth Syst. Dyn.* **5**, 409–422 (2014).
24. Tokarska, K. B., Gillett, N. P., Weaver, A. J., Arora, V. K. & Eby, M. The climate response to five trillion tonnes of carbon. *Nat. Clim. Change* **6**, 851–855 (2016).
25. Eby, M. et al. Historical and idealized climate model experiments: an intercomparison of Earth system models of intermediate complexity. *Clim. Past* **9**, 11–1140 (2013).
26. Pfister, P. L. & Stocker, T. F. State-dependence of the climate sensitivity in earth system models of intermediate complexity. *Geophys. Res. Lett.* **44**, 643–10,653 (2017).
27. Zickfeld, K., Arora, V. K. & Gillett, N. P. Is the climate response to carbon emissions path dependent? *Geophys. Res. Lett.* **39**, L05703 (2012).
28. Arora, V. K. et al. Carbon-concentration and carbon-climate feedbacks in CMIP5 Earth system models. *J. Clim.* **26**, 5289–5314 (2013).
29. Arora, V. K. et al. Carbon-concentration and carbon-climate feedbacks in CMIP6 models, and their comparison to CMIP5 models. *Biogeosci. Discuss.* **2019**, 1–124 (2019).
30. Keller, D. P. et al. The carbon dioxide removal model intercomparison project (CDRMIP): rationale and experimental protocol for CMIP6. *Geosci. Model Dev.* **11**, 1133–1160 (2018).
31. Eyring, V. et al. Overview of the coupled model intercomparison project phase 6 (CMIP6) experimental design and organization. *Geosci. Model Dev.* **9**, 1937–1958 (2016).

Publisher's note Springer Nature remains neutral with regard to jurisdictional claims in published maps and institutional affiliations.

© The Author(s), under exclusive licence to Springer Nature Limited 2021

Methods

Model description. We use the UVic ESCM, a model of intermediate complexity with a horizontal grid resolution of 1.8° (meridional) $\times 3.6^\circ$ (zonal) (ref. ⁹). The version of the UVic ESCM used here (2.9) (ref. ¹⁰) includes a three-dimensional (3D) ocean general circulation model with isopycnal mixing and a Gent–McWilliams parameterization of the effect of eddy-induced tracer transport. For diapycnal mixing, a Bryan and Lewis profile of diffusivity is applied, with a value of $0.3 \times 10^{-4} \text{ m}^2 \text{ s}^{-1}$ in the pycnocline. The ocean model is coupled to a dynamic–thermodynamic sea-ice model and a single-layer energy–moisture balance model of the atmosphere with dynamical feedbacks⁹. The model includes a parameterization of water vapour/planetary longwave feedbacks, and the radiative forcing associated with changes in atmospheric CO₂ and other greenhouse gases is prescribed as a modification of the planetary longwave radiative flux⁹. The land surface and vegetation are represented by a simplified version of the Hadley Centre's Met Office Surface Exchange Scheme coupled to the dynamic vegetation model Top-down Representation of Interactive Foliage and Flora Including Dynamics³². Ocean carbon is simulated by means of an Ocean Carbon Cycle Model Intercomparison Project-type inorganic carbon-cycle model and a marine ecosystem/biogeochemistry model solving prognostic equations for nutrients, phytoplankton, zooplankton and detritus³³. The version of the UVic ESCM used here includes a marine sediment component. The UVic ESCM has been included in numerous model intercomparison projects, including the Earth System Model of Intermediate Complexity Intercomparison in support of the Fifth Assessment Report of the Intergovernmental Panel on Climate Change^{10,25}. The model's standard climate sensitivity is 3.5°C for a doubling of the pre-industrial atmospheric CO₂ concentration²⁵. In terms of the carbon-cycle response to CO₂ and climate change, the UVic ESCM lies in the middle of the range of responses of Earth systems models of intermediate complexity and complex Earth system models^{25,28}.

Experimental design. The UVic ESCM was spun up under different atmospheric CO₂ concentrations: 1×, 1.5×, 2×, 3× and 4× the pre-industrial CO₂ concentration of 284 ppm. Each spin-up simulation was run for 10,000 years until the drift in ocean tracers was negligible. Positive and negative CO₂ emission pulses of different magnitude (100 GtC, 200 GtC, 500 GtC and 1,000 GtC) were then applied from these equilibrium states. In applying negative CO₂ emissions, the removed CO₂ is taken out of the system permanently. This is akin to direct air capture technology whereby CO₂ is directly removed from the atmosphere and stored underground or made into permanent products. In all simulations, non-CO₂ (anthropogenic and natural) radiative forcings were held fixed at their pre-industrial level.

Biogeochemically coupled simulations. For an initial state at equilibrium with twice the pre-industrial atmospheric CO₂ concentration ($2\times\text{CO}_2$), we conducted a set of biogeochemically coupled pulse simulations³⁸, whereby the radiative forcing from CO₂ was fixed at pre-industrial levels. In these simulations, the land and ocean carbon cycle components 'see' evolving atmospheric CO₂ concentrations, but do not experience climate changes associated with these evolving concentrations. They do, however, experience small climate changes associated with biophysical effects of vegetation changes³⁹. These simulations serve to isolate biogeochemical from climate effects of changing atmospheric CO₂ concentration on the carbon cycle.

Simulations initialized from a transient state. In addition to pulse simulations initialized from equilibrium states, we conducted a set of simulations whereby positive and negative CO₂ pulses were applied from a transient $2\times\text{CO}_2$ state. This state was reached along a trajectory of atmospheric CO₂ concentrations increasing at 1% per year from pre-industrial levels over 70 years. We also conducted a simulation with zero CO₂ emissions initialized from this transient state. The difference between the pulse simulations initialized from the transient state and the zero-emissions simulation allowed us to isolate the response to the emission pulses from the response to the increasing atmospheric CO₂ concentration prior to the pulse release.

Simulations with different emission rates. To test the robustness of the C–CC response against the rate of CO₂ emission/removal, we conducted a set of simulations with positive and negative emissions of 100 GtC, 500 GtC and 1,000 GtC emitted/removed at a rate of 10 GtC per year from a $2\times\text{CO}_2$ equilibrium state. The response in these simulations is compared with that in the simulations with instantaneous (pulse) emissions/removals initialized from the same state.

Revelle factor calculation. The Revelle factor shown in the Supplementary Figures was calculated from simulated sea surface values of dissolved inorganic carbon,

pH, temperature, salinity and phosphate, using the MATLAB version of the CO2SYS program^{34,35} with the dissociation constants for carbonic acid (H₂CO₃) and bicarbonate (HCO₃⁻) of Mehrbach et al.³⁶ refitted by Dickson and Millero³⁷ and the dissociation constants for potassium bisulphate (KHSO₄⁻) of Dickson³⁸.

Data availability

The UVic ESCM data underlying this study are available at <https://doi.org/10.5281/zenodo.4641434> (ref. ³⁹). Source data are provided with this paper.

Code availability

The code for UVic ESCM version 2.9 is available at <http://terra.seos.uvic.ca/model/2.9/>.

References

32. Meissner, K. J., Weaver, A. J., Matthews, H. D. & Cox, P. M. The role of land surface dynamics in glacial inception: a study with the UVic Earth system model. *Clim. Dyn.* **21**, 515–537 (2003).
33. Schmittner, A., Oschlies, A., Matthews, H. D. & Galbraith, E. D. Future changes in climate, ocean circulation, ecosystems and biogeochemical cycling simulated for a business-as-usual CO₂ emission scenario until year 4000 AD. *Glob. Biogeochem. Cycles* **22**, L19703 (2008).
34. van Heuven, S., Pierrot D., Rae, J. W. B., Lewis, E. & Wallace, D. W. R. MATLAB program developed for CO₂ system calculations, ORNL/CDIAC-105 (Carbon Dioxide Information Analysis Center, Oak Ridge National Laboratory, 2011).
35. Lewis, E. & Wallace, D. W. R. Program developed for CO₂ system calculations, ORNL/CDIAC-105 (Carbon Dioxide Information Analysis Center, Oak Ridge National Laboratory, 1998).
36. Mehrbach, C., Culberson, C. H., Hawley, J. E. & Pytkowicz, R. Measurement of the apparent dissociation constants of carbonic acid in seawater at atmospheric pressure. *Limnol. Oceanogr.* **18**, 897–907 (1973).
37. Dickson, A. G. & Millero, F. J. A comparison of the equilibrium constants for the dissociation of carbonic acid in seawater media. *Deep Sea Res. A* **34**, 1733–1743 (1987).
38. Dickson, A. G. Standard potential of the reaction: AgCl(s) + 12H₂(g) = Ag(s) + HCl(aq) and the standard acidity constant of the ion HSO₄⁻ in synthetic seawater from 273.15 to 318.15 K. *J. Chem. Thermodyn.* **22**, 113–127 (1990).
39. Zickfeld, K. & Azevedo, D. Asymmetry in the climate-carbon cycle response to positive and negative CO₂ emissions version 1 (2021); <https://doi.org/10.5281/zenodo.4641434>

Acknowledgements

K.Z. and S.M. acknowledge support from the Natural Sciences and Engineering Research Council (NSERC) Discovery Grant Program. D.A. was partly supported by the NSERC USRA Program. This research was enabled in part by computing resources provided by Westgrid and Compute Canada.

Author contributions

K.Z. conceived the study, designed the model experiments, analysed and interpreted the model data and wrote the manuscript. D.A. performed the model simulations and contributed to the model data analysis and interpretation. S.M. provided analyses for the ocean response and contributed to the interpretation of results. H.D.M. provided suggestions for additional analysis and manuscript revisions.

Competing interests

The authors declare no competing interests.

Additional information

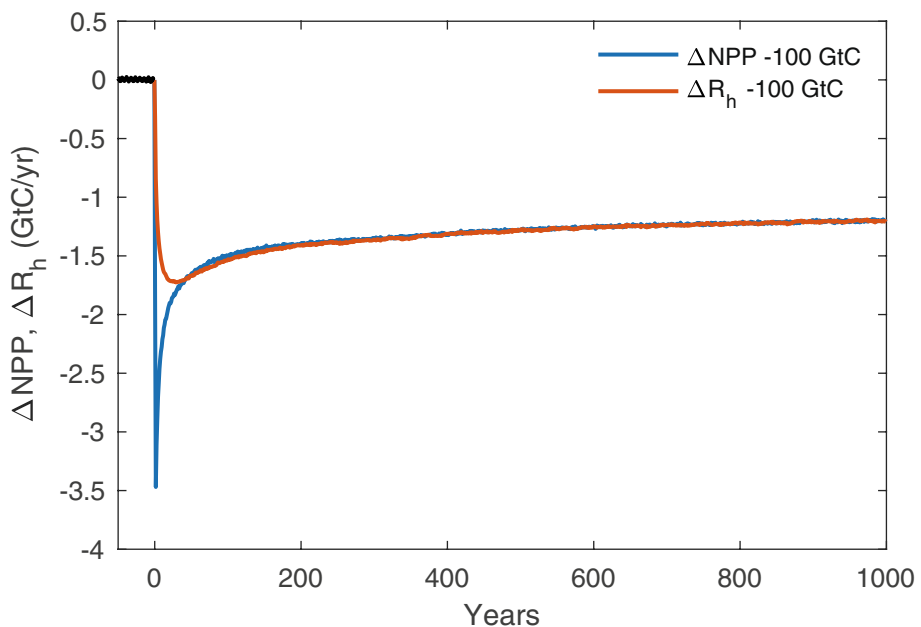
Extended data is available for this paper at <https://doi.org/10.1038/s41558-021-01061-2>.

Supplementary information The online version contains supplementary material available at <https://doi.org/10.1038/s41558-021-01061-2>.

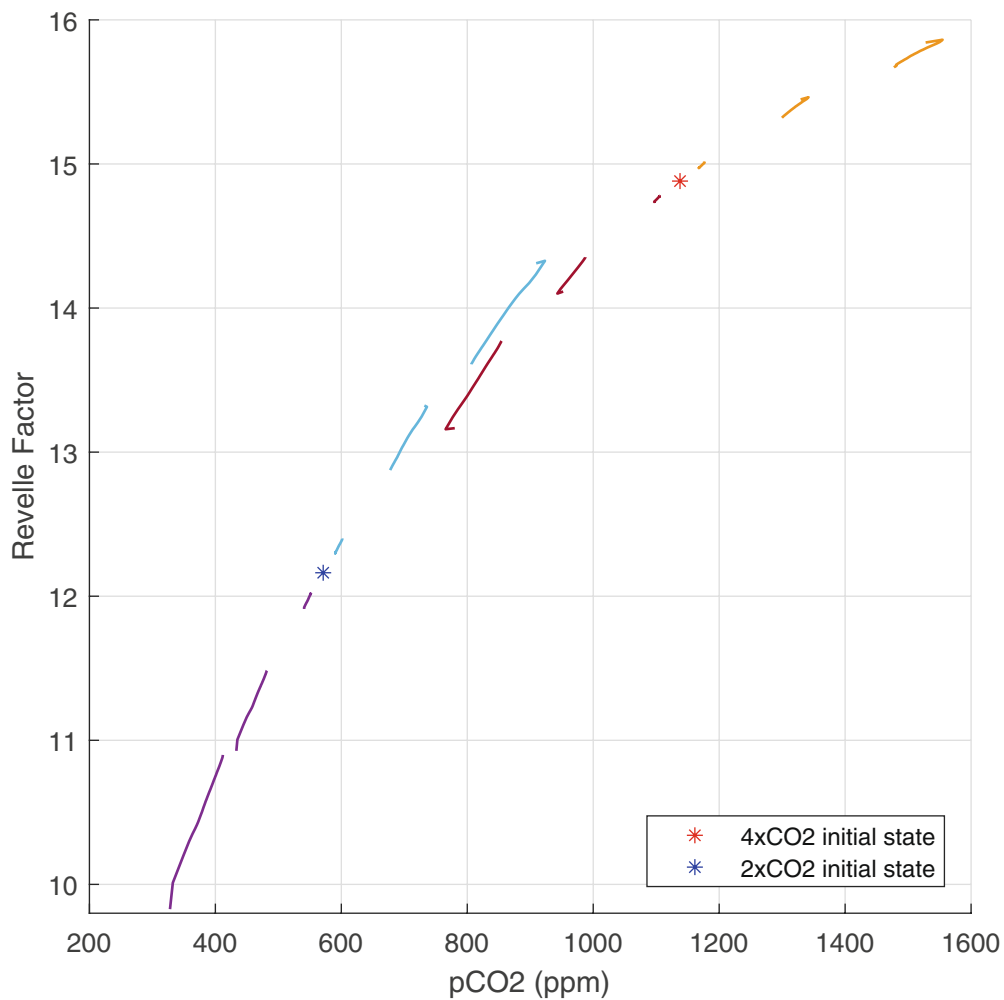
Correspondence and requests for materials should be addressed to K.Z.

Peer review information *Nature Climate Change* thanks Jörg Schwinger and the other, anonymous, reviewer(s) for their contribution to the peer review of this work.

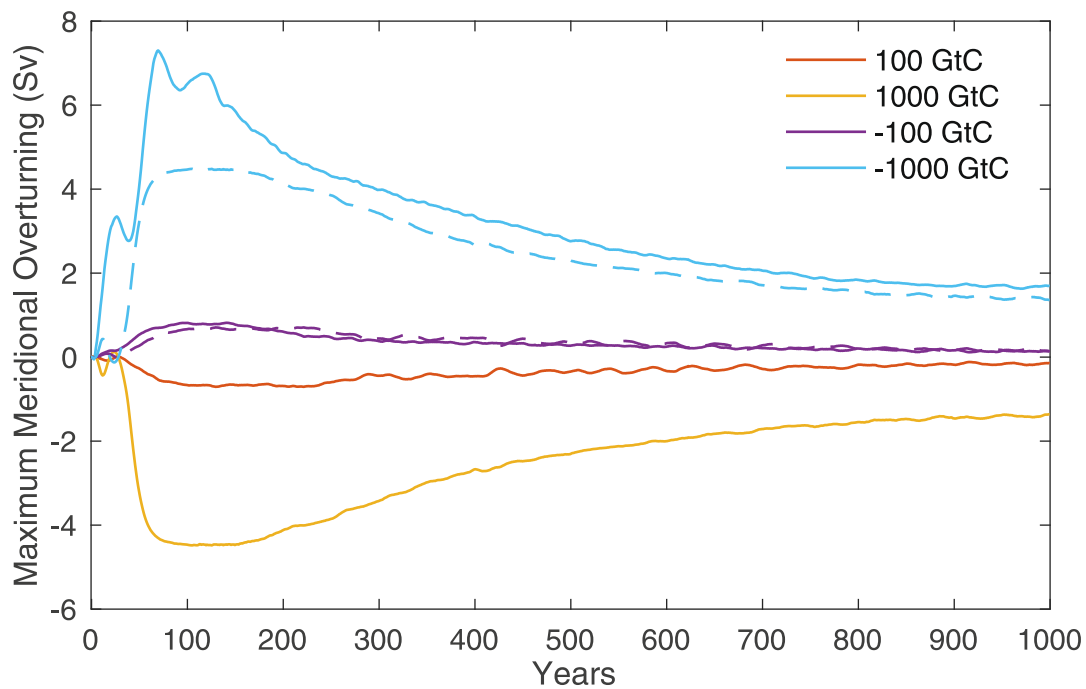
Reprints and permissions information is available at www.nature.com/reprints.



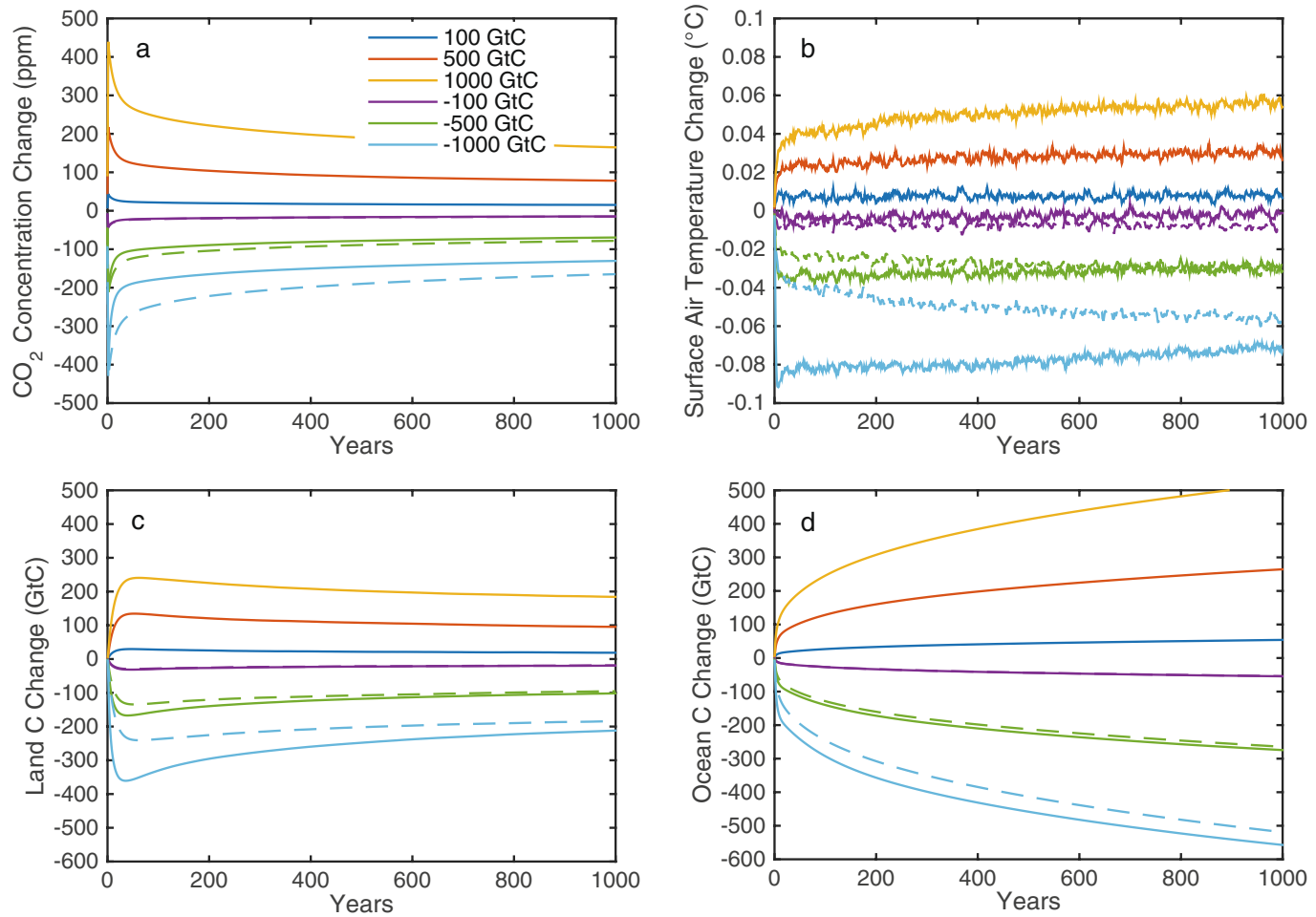
Extended Data Fig. 1 | Response of land carbon fluxes to CO₂ removal. Change in net primary productivity (NPP) and soil respiration (Rh) for a 100 GtC removal applied from a state in equilibrium with twice the pre-industrial atmospheric CO₂ concentration (2xCO₂). Changes are calculated relative to a control simulation with zero CO₂ emissions.



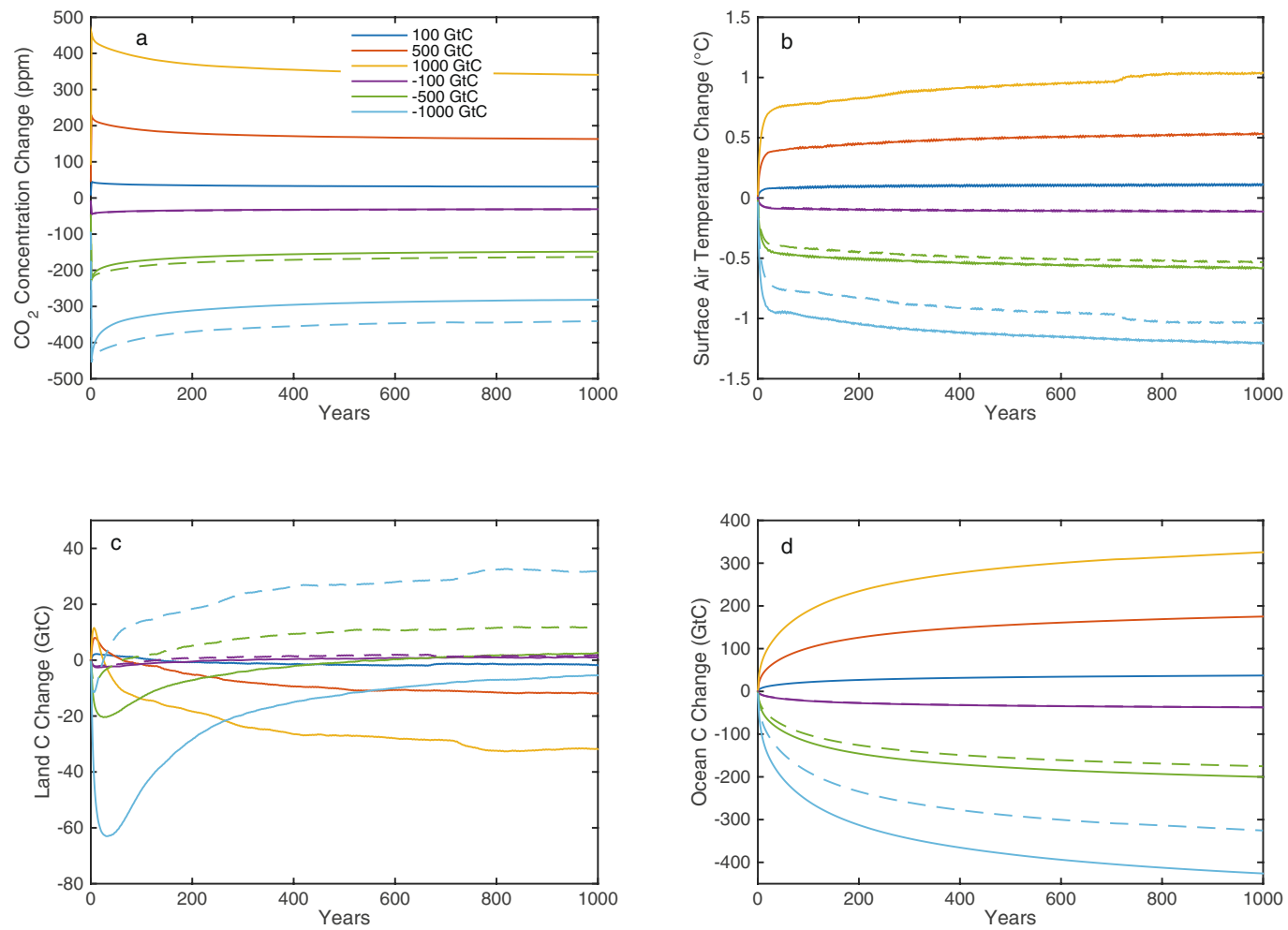
Extended Data Fig. 2 | Revelle factor. Revelle factor as function of surface ocean CO₂ partial pressure (pCO₂) for simulations with pulses of different magnitude (± 100 GtC, ± 500 GtC, ± 1000 GtC) applied from 2xCO₂ (cold colors) and 4xCO₂ (warm colors) initial states. The Revelle factor is a measure of the ocean's buffer capacity. It is inversely related to the buffer capacity; that is, a higher Revelle factor indicates a lower buffer capacity and vice versa.



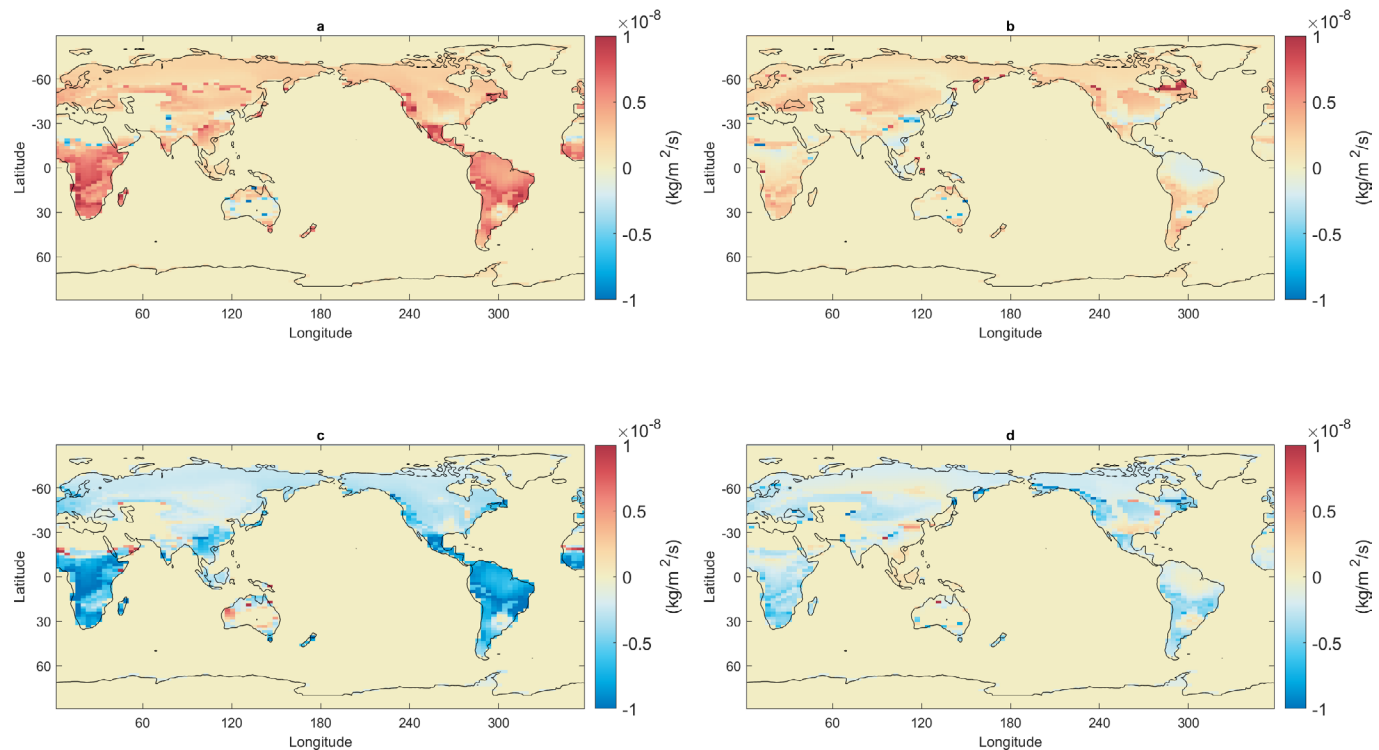
Extended Data Fig. 3 | Meridional overturning circulation response to CO₂ emissions and removals. Change in maximum meridional overturning streamfunction for pulse emissions/removals of ± 100 GtC and ± 1000 GtC applied from a $2\times\text{CO}_2$ initial state. Changes are calculated relative to a control simulation with zero CO₂ emissions. Dashed lines show the response to positive CO₂ emissions mirrored about the horizontal zero-axis to illustrate asymmetries in the response.



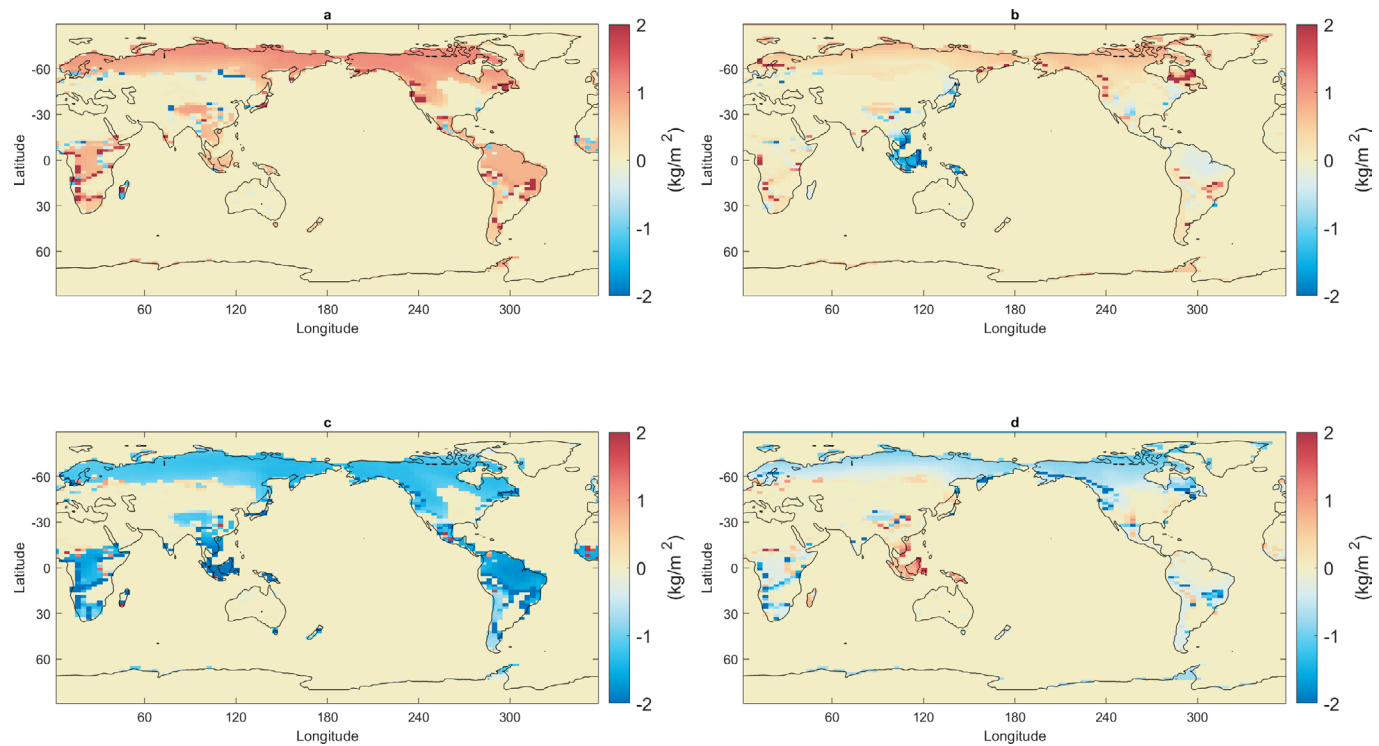
Extended Data Fig. 4 | Carbon cycle and temperature response to CO₂ emissions and removals in biogeochemically coupled simulations. Carbon cycle and surface air temperature responses to positive and negative CO₂ emission pulses as simulated in the biogeochemically coupled simulations (see Methods). Pulse emissions and removals are applied from a 2×CO₂ initial state. **(a)**, Atmospheric CO₂ concentration anomaly, **(b)** surface air temperature anomaly, **(c)** land carbon storage change, **(d)** ocean carbon storage change. Changes are calculated relative to a control simulation with zero CO₂ emissions. Dashed lines show the response to positive CO₂ emission pulses mirrored about the horizontal zero-axis to illustrate asymmetries in the responses.



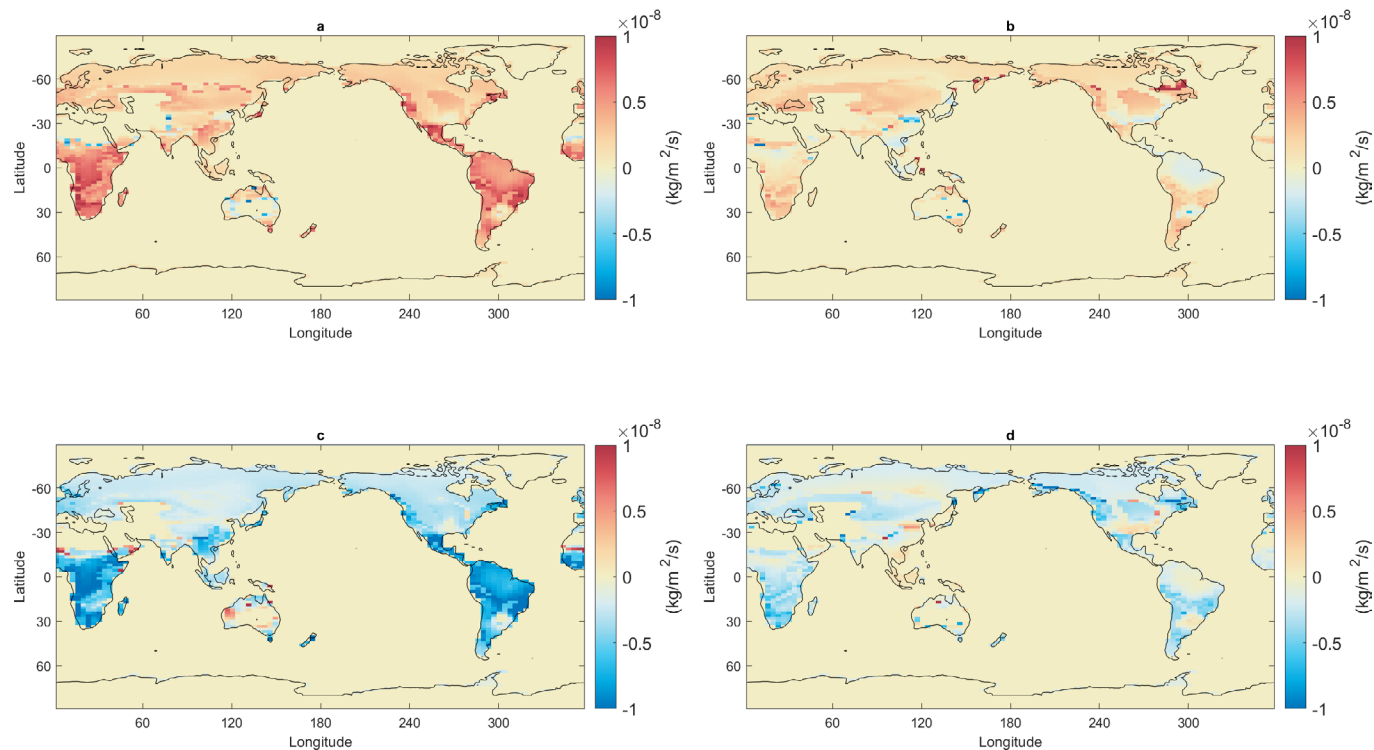
Extended Data Fig. 5 | Carbon cycle and temperature response to CO₂ emissions and removals applied from a 4xCO₂ state. Carbon cycle and temperature responses to positive and negative CO₂ emission pulses of different magnitude applied from a state at equilibrium with four times the pre-industrial atmospheric CO₂ concentration (4xCO₂). **(a)**, Atmospheric CO₂ concentration anomaly, **(b)** surface air temperature anomaly, **(c)** land carbon storage change, **(d)** ocean carbon storage change. Changes are calculated relative to a control simulation with zero CO₂ emissions initialized from the 4xCO₂ equilibrium state. Dashed lines show the response to positive CO₂ emission pulses mirrored about the horizontal zero-axis to illustrate asymmetries in the responses.



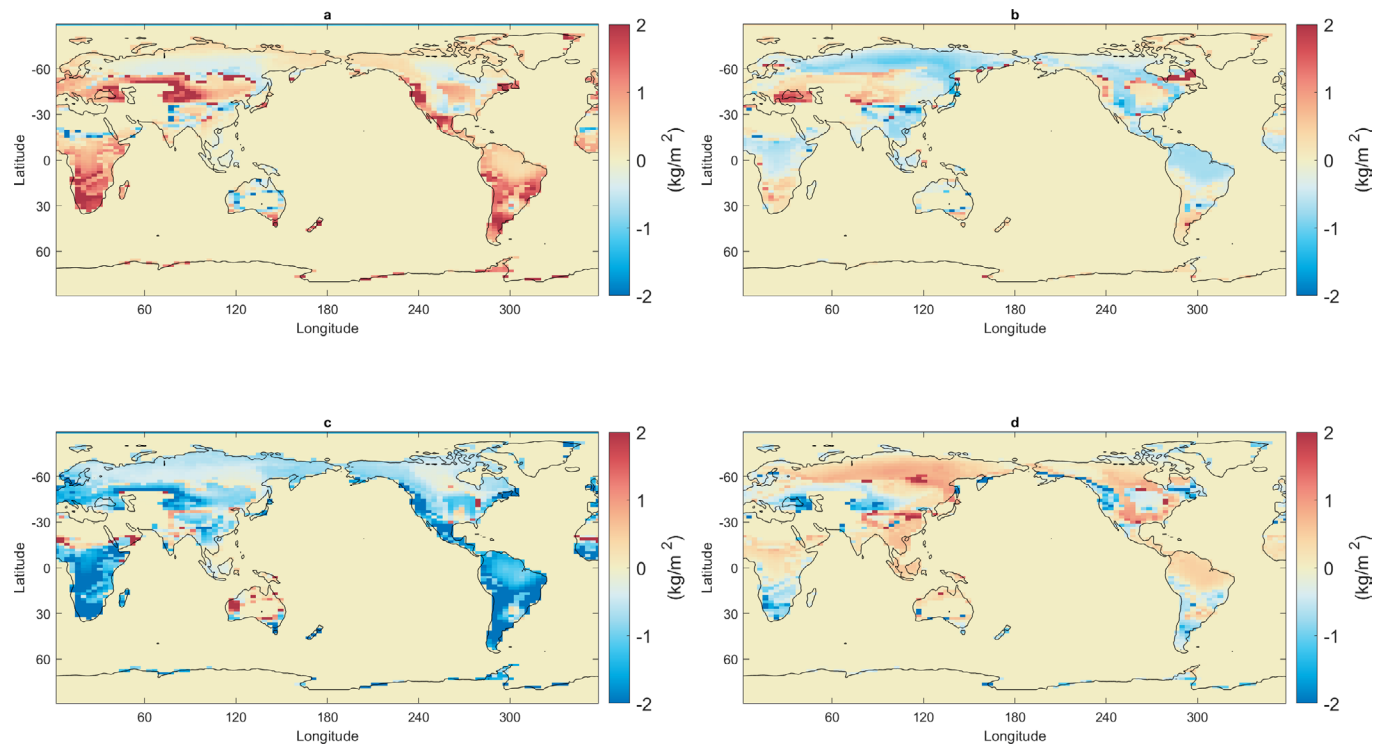
Extended Data Fig. 6 | Changes in net primary productivity 100 years after CO₂ pulse release. (a) 1000 GtC pulse applied from a 2×CO₂ initial state, (b) 1000 GtC pulse applied from a 4×CO₂ initial state, (c) -1000 GtC pulse applied from a 2×CO₂ initial state, (d) -1000 GtC pulse applied from a 4×CO₂ initial state. Changes are calculated relative to a control simulation with zero CO₂ emissions initialized from a 2×CO₂ (panels a, c) or 4×CO₂ equilibrium state (panels b, d).



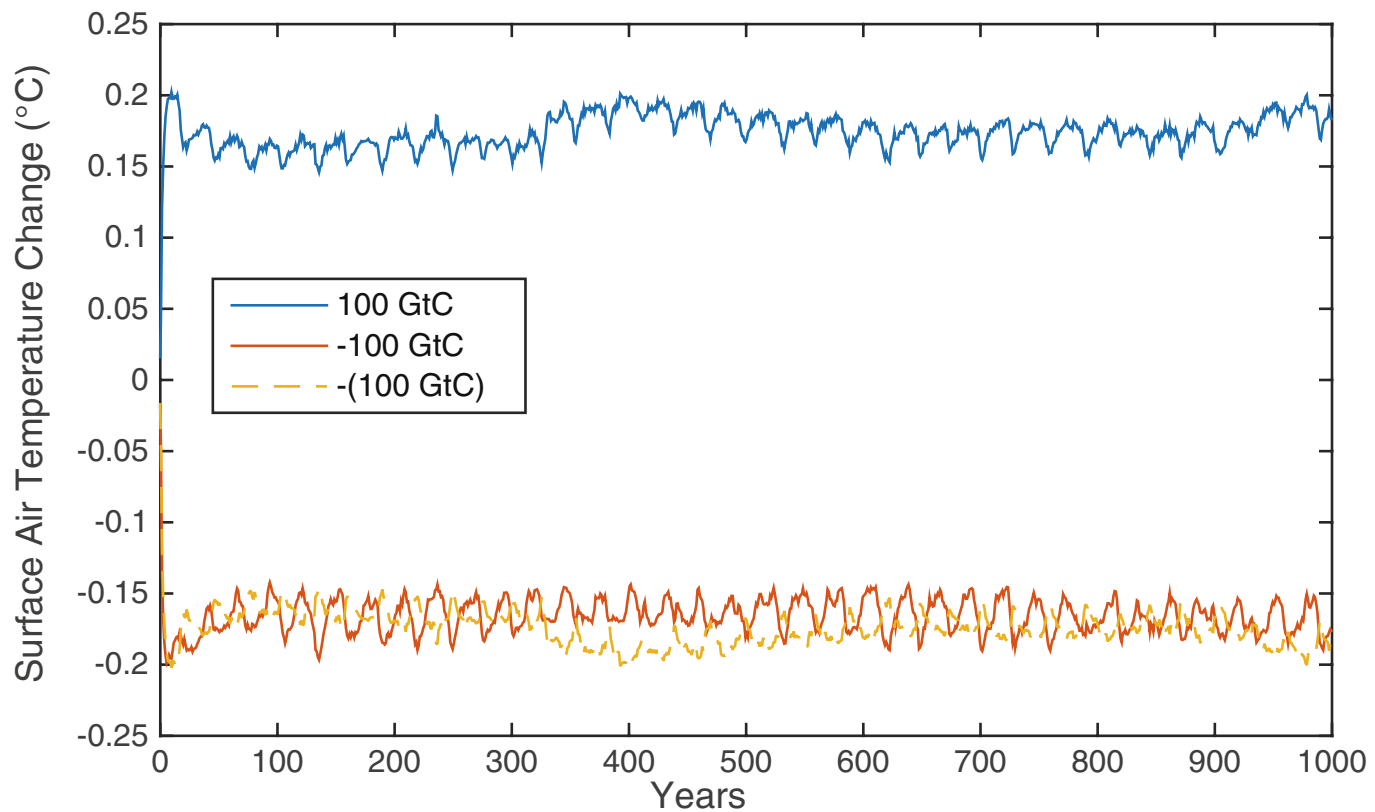
Extended Data Fig. 7 | Spatial changes in vegetation carbon 100 years after CO_2 pulse release. Changes in vegetation carbon 100 years after CO_2 pulse release. (a), 1000 GtC pulse applied from a $2\times\text{CO}_2$ initial state, (b) 1000 GtC pulse applied from a $4\times\text{CO}_2$ initial state, (c) -1000 GtC pulse applied from a $2\times\text{CO}_2$ initial state, (d) -1000 GtC pulse applied from a $4\times\text{CO}_2$ initial state. Changes are calculated relative to a control simulation with zero CO_2 emissions initialized from a $2\times\text{CO}_2$ (panels a, c) or $4\times\text{CO}_2$ equilibrium state (panels b, d).



Extended Data Fig. 8 | Spatial changes in soil respiration 100 years after CO₂ pulse release. Changes in soil respiration 100 years after CO₂ pulse release. (a) 1000 GtC pulse applied from a 2×CO₂ initial state, (b) 1000 GtC pulse applied from a 4×CO₂ initial state, (c) -1000 GtC pulse applied from a 2×CO₂ initial state, (d) -1000 GtC pulse applied from a 4×CO₂ initial state. Changes are calculated relative to a control simulation with zero CO₂ emissions initialized from a 2×CO₂ (panels a, c) or 4×CO₂ equilibrium state (panels b, d).



Extended Data Fig. 9 | Spatial changes in soil carbon 100 years after CO_2 pulse release. Changes in soil carbon 100 years after CO_2 pulse release. (a), 1000 GtC pulse applied from a $2\times\text{CO}_2$ initial state, (b) 1000 GtC pulse applied from a $4\times\text{CO}_2$ initial state, (c) -1000 GtC pulse applied from a $2\times\text{CO}_2$ initial state, (d) -1000 GtC pulse applied from a $4\times\text{CO}_2$ initial state. Changes are calculated relative to a control simulation with zero CO_2 emissions initialized from a $2\times\text{CO}_2$ (panels a, c) or $4\times\text{CO}_2$ equilibrium state (panels b, d).



Extended Data Fig. 10 | Variability in surface air temperature response. Variability in the surface air temperature response to a positive and negative 100 GtC CO₂ emission pulse applied from a state in equilibrium with the pre-industrial atmospheric CO₂ concentration (1xCO₂). The dashed line shows the response to the positive CO₂ emission pulse mirrored about the horizontal zero-axis to illustrate the asymmetry in the response. Temperature variability in the model arises due to variability in the ocean-sea ice system.